Acta Astronautica 176 (2020) 204–215

Contents lists available at ScienceDirect

Acta Astronautica

journal homepage: www.elsevier.com/locate/actaastro

Data quality assessment of Diffusion Coefficient Measurements in ternary mIXtures 4 (DCMIX4) experiment

Aliaksandr Mialdun[a], Mounir M. Bou-Ali[b], Marco Braibanti[c], Fabrizio Croccolo[d], Ane Errarte[b], José Miguel Ezquerro[e], José Javier Fernández[e], Loreto García-Fernández[f,g], Quentin Galand[a], Yuri Gaponenko[a], Fina Gavaldà[h], Werner Köhler[i], Tatyana Lyubimova[j], José María Ortiz de Zárate[k], Jacobo Rodríguez[e], Xavier Ruiz[h], Ilya I. Ryzhkov[l,m], Marcel Schraml[i], Valentina Shevtsova[a], Stephan Van Vaerenbergh[a], Viktar Yasnou[a], Henri Bataller[d,*]

[a] MRC, CP 165/62, Université libre de Bruxelles (ULB), 50, Ave. F.D. Roosevelt, B-1050, Brussels, Belgium
[b] Mechanical and Manufacturing Department, Mondragon Goi Eskola Politeknikoa (MGEP), Loramendi 4, Apdo. 23, 20500, Mondragon, Spain
[c] European Space Agency (ESA), ESTEC, Noordwijk, the Netherlands
[d] Universite de Pau et des Pays de l'Adour, E2S UPPA, CNRS, TOTAL, LFCR UMR5150, Anglet, France
[e] E-USOC, Ciencias y Operaciones Espaciales, Center for Computational Simulation, Escuela Técnica Superior de Ingeniería Aeronáutica y del Espacio, Universidad Politécnica de Madrid, Plaza Cardenal Cisneros 3, 28040 Madrid, Spain
[f] Centre National d'Etudes Spatiales, 2 Place Maurice Quentin, 75001, Paris, France
[g] Facultad de Farmacia, Universidad CEU San Pablo, Urbanización Montepríncipe, Boadilla del Monte, E-28668, Madrid, Spain
[h] Department of Química Física i Inorgànica, Universitat Rovira i Virgili, Tarragona, Spain
[i] Physikalisches Institut, Universität Bayreuth, 95440, Bayreuth, Germany
[j] Institute of Continuous Media Mechanics UB RAS, 614013, Perm, Russia
[k] Departamento de Estructura de la Materia, Física Térmica y Electrónica, Facultad de Ciencias Físicas, Universidad Complutense de Madrid, Plaza de las Ciencias 1, 28040, Madrid, Spain
[l] Institute of Computational Modelling SB RAS, FRC KSC SB RAS, Akademgorodok, 660036, Krasnoyarsk, Russia
[m] Siberian Federal University, Krasnoyarsk, 660041 Russia

ARTICLE INFO

Keywords:
International space station
Thermodiffusion
Ternary mixtures
Phase-shifting interferometry
Thermal regulation stability

ABSTRACT

Thermodiffusion, which leads to a component separation in a mixture due to the thermal gradient, still does not have an unambiguous microscopic picture. Therefore, experimental studies, especially in convection free environment, are important. As part of the 4th campaign on the DCMIX project, thermodiffusion experiments on three compositions of the toluene-methanol-cyclohexane ternary mixture, on a mixture of fullerene-tetralin-toluene and on a mixture of polystyrene-toluene-cyclohexane have been performed in microgravity conditions on board the International Space Station. A binary mixture of polystyrene-toluene has been filled into the companion cell for the campaign. The Selectable Optical Diagnostics Instrument (SODI), wich is a two-wavelength Mach-Zehnder interferometer for the ternary mixtures, plus a monochromatic Mach-Zehnder interferometer for the binary mixture, has been used in order to obtain the temperature and the concentration fields in the cells. Precisely, it is a 5-steps phase-shifting interferometry technique which is implemented with SODI, producing by means of laser illumination a set of 5 phase-shifted images of $\pi/2$ between them as function of the time. A total of 58 runs of various durations and at different mean temperatures have been conducted. Here, we evaluate the contrast of the interferograms, the quality in the phase stepping, the stability of the thermal regulation of the experiments and the level of environmental disturbances on board the space station during the campaign.

1. Introduction

The aim of the Diffusion Coefficient Measurements in ternary mIXtures (DCMIX) project is to perform, in gravity-free environment thermodiffusion experiments, in order to provide quantitative measurements of mass diffusion and Soret coefficients on ternary mixtures

* Corresponding author.
E-mail address: henri.bataller@univ-pau.fr (H. Bataller).

https://doi.org/10.1016/j.actaastro.2020.06.020
Received 31 May 2020; Accepted 9 June 2020
Available online 17 June 2020

of different origins. These series of experiments are performed on board the International Space Station (ISS) making use of the Selectable Optical Diagnostics Instrument (SODI) installed within the Microgravity Science Glovebox (MSG) inside the Destiny U.S. Laboratory of the ISS. The instrument comprises a two-wavelength (670 nm and 935 nm) Mach-Zehnder interferometer (MZI) with the possibility to change alignment and magnification. It provides the possibility to measure diffusion and Soret coefficients in binary and ternary mixtures. It is recognized that it is impossible to perform very extensive and systematic thermodiffusion studies in a microgravity environment due to the naturally limited availability of experiment time. With present technology, the coverage of the full ternary composition diagram of a single ternary system on a dense grid would require measurement times on the order of years. This is why the improvement of the reliability and the understanding of ground based measurements has always been considered an important objective of the DCMIX project. For flight experiments, 5 ternary and 1 binary mixtures can be studied at the same time, delivered to the ISS in the form of a cell array pre-filled with the liquid samples. Within the framework of the DCMIX project, four measurement campaigns were carried out on the ISS.

The first campaign, DCMIX1, was completed in January 2012. The samples were ternary mixtures of three hydrocarbons (tetralin, isobutylbenzene and dodecane). These compounds serve as model systems for the oil industry and the associated binaries are known as the so-called Fontainebleau benchmark systems. An experimental benchmark study was organised comparing ground and microgravity results at the point with mass fractions 0.80/0.10/0.10 for the ternary mixture THN-IBB-C12 [1]. A large part of the DCMIX team was involved in processing of the selected runs [2].

The second campaign, DCMIX2, was completed in January 2014. The ternary mixtures were composed of toluene, methanol and cyclohexane. This system is of particular interest due to the existence of a miscibility gap and a consolute critical point. Its investigation in ground based experiments is significantly more complex than in case of the DCMIX1 mixtures due to double diffusive convective instabilities [3]. It was shown that Soret separation increases at least by one order of magnitude towards the demixing zone. An unexpected experimental result was obtained in the binary cell filled with a toluene-cyclohexane mixture: the thermodiffusion coefficient D_T is temperature independent for this mixture [4]. For the ternary mixture a linear dependence of the Soret coefficients on temperature was established. Processing the same set of images by different teams showed that the results depend on the methodology used to obtain the optical phase [5]. Furthermore, a small discrepancy in the optical phase (≈10%–15%) can lead to a large discrepancy between the results due to the propagation of errors at the state points with poor optical contrasts and/or ill-conditioned contrast factor matrices.

DCMIX3 was originally scheduled to be brought to the ISS in October 2014. Unfortunately, due to the catastrophic failure of the CRS Orb-3 mission during lift off, the first cell array was lost. A second cell array was built and successfully delivered to the ISS aboard SpaceX CRS-9 in July 2016. Experiments were completed on 17 November 2016. The DCMIX3 samples were ternary mixtures of water, ethanol, and triethylene glycol, for which a sign change of the Soret coefficient along the binary water-ethanol boundary was already known from the literature. Motivated by the microgravity experiments, a second sign change was discovered along the ethanol-triethylene glycol boundary in accompanying laboratory experiments. Sign changes of the Soret coefficient render these mixtures particularly sensitive to unwanted convective instabilities under gravity conditions. For the mixture of symmetric composition with equal mass fractions it has been possible to obtain consistent results between the microgravity measurements and the laboratory ground experiments performed with optical beam deflection and with a thermogravitational column [6]. The evaluation of the other cells has not yet been finished. 5-steps phase-shifting

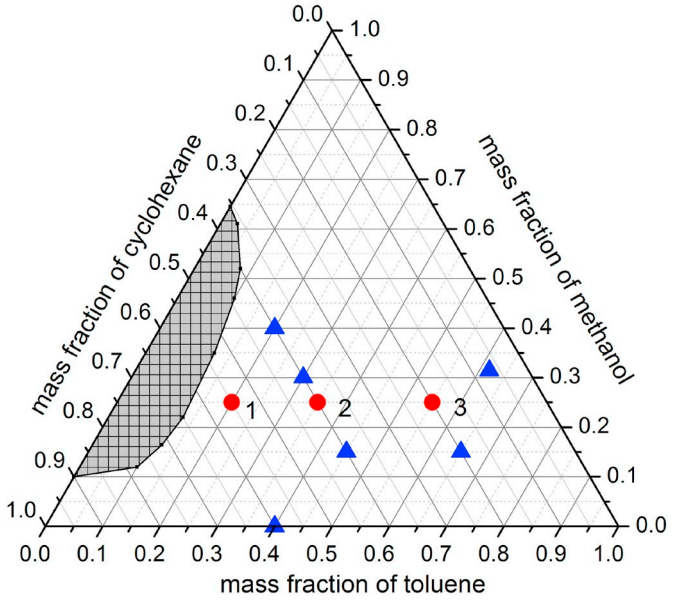

Fig. 1. Toluene-methanol-cyclohexane concentration diagram indicating DCMIX4 cells 1–3 composition (red circles) and as a reminder of DCMIX2 samples composition (blue triangles). The hatched area indicates demixing zone at T = 25 °C; the demixing zone expands as long as the temperature decrease. (For interpretation of the references to color in this figure legend, the reader is referred to the Web version of this article.)

interferometry technique relies on acquiring a set of 5 images with $\pi/2$ phase shift between them, which is called a stack. Some of the DCMIX3 measurements were affected by laser instabilities that render the standard phase stepping evaluation procedure impossible. A new evaluation scheme, which is based on single image analysis, has been developed, which allows evaluating also the malformed image stacks without information loss. This alternative technique proves the robustness of the SODI instrument, which can deliver valid data even in situations where some components of the instrument fail to work as designed [7].

For the 4th campaign of the project, which is the subject of this work, the scientific team wanted to maximize the scientific return of the mission by maximizing on the diversity of the chemical systems sent into space. Taking into account novelty and importance of the obtained results for the ternary mixture, three cells of DCMIX4 (1–3) have been filled with toluene-methanol-cyclohexane mixtures at concentrations different from those of DCMIX2 and closer to phase separation, in order to confirm the slowing-down of the mass diffusion and the divergence of the Soret coefficients. In Fig. 1 the ternary composition map is reported. All three mixtures have the same content of methanol (25% by mass). The composition of the first cell is the one closer to the demixing zone (shown as the shaded area) at small toluene concentration. The analysis of the cells 1–3 has been coordinated by the team headed by V. Shevtsova (VS), from Université libre de Bruxelles (ULB), Belgium. Another sample of DCMIX4 includes a mixture of fullerene (C60)-tetralin-toluene, as the first complex mixture including nanoparticles [8]. The results obtained by measuring this sample are expected to provide added value and a high impact in this very active research area with so many applications: advanced manufacturing, health, nanotechnologies and biotechnology [9]. The study of the cell 4 has been coordinated by the team headed by M.M. Bou-Ali (MMBA), from Mondragon Goi Eskola Politeknikoa (MGEP), Spain. The ternary mixture of polystyrene-toluene-cyclohexane has been chosen mainly because the two eigenvalues of the mass diffusion coefficients matrix are expected to be well separated, by a factor of about 10, as this mixture includes a polymer as one of the components, namely the polystyrene, having a much larger molecular weight than the other two [10–12]. This implies that the time evolution of the concentration profiles measured by SODI two-

Table 1
List of liquid mixtures selected for the DCMIX4 cell array. The name of the coordinator is written after the cell number. Compositions of ternary mixtures are given in percent mass fractions.

Cell #	Component 1	Component 2	Component 3
1 (VS)	toluene	methanol	cyclohexane
	20	25	55
2 (VS)	toluene	methanol	cyclohexane
	35	25	40
3 (VS)	toluene	methanol	cyclohexane
	55	25	20
4 (MBA)	fullerene*	tetralin	toluene
	0.07	60	39.93
5 (HB, FC)	Polystyrene**	toluene	cyclohexane
	2	39	59
6 (HB, FC)	Polystyrene**	toluene	–
	2	98	–

*C60 **MW 4730 g/mol.

wavelength diagnostics will be easier to analyse and interpret, as the different contributions can be also separated on the basis of their kinetics. A binary mixture of polystyrene-toluene completes the cell array in order to establish reference values for the polymer in a molecular solvent. The analysis of cells 5–6 has been carried out by the team headed by H. Bataller (HB) and F. Croccolo (FC) from Université de Pau et des Pays de l'Adour (UPPA), France. The sample content of all the cells is detailed in Table 1. For component numbering, a hydrodynamic approach has been adopted, corresponding to a decreasing order of density; i.e. component 1 is the denser one and so on.

The liquids are placed into quartz Soret cells of 0.5 ml (5 mm (H) x 10 mm (L) x 10 mm (W)). The smallest dimension is in the direction of the thermal gradient. These cells are combined in a cell array that contains five such cells, called primary, with ternary mixtures and one, called companion cell, with the binary mixture. The cell array was delivered to the ISS inside the unmanned Cygnus cargo ship launched by the Antares rocket on 17th November 2018. It was installed inside SODI on Wednesday 12th December 2018 by the NASA astronaut Serena Auñon-Chancellor. The first scientific experiment started on 13th December 2018 and the tests continued until 4th March 2019. All the experiments were handled by the Spanish User Support and Operations Center (EUSOC) in Madrid. During the campaign, a report was written on the good progress of the experiment and on the basis of the downloaded telemetry data [13]. To date, all of the stacks have been collected and made available to the scientific team. Under the coordination of ESA, the first task for the scientific team was to assess the quality of the data in order to identify failing runs and make recommendations for future data processing. In this article we report this work of data quality assessment.

2. Experiment description

2.1. Selectable Optical Diagnostics Instrument

The DCMIX experiments rely on optical probing of refractive index changes in order to infer time resolved spatial composition changes. Since ternary mixtures are described by two independent composition variables, the use of two different readout wavelegths is needed. SODI consist of a two-color MZI equipped with two lasers operating at 670 nm and 935 nm (designated MR and MN for Moving Red and Moving Near-infrared) that probes successively the primary cells. For the binary mixtures there is only one independent composition variable. SODI holds in addition a monochromatic MZI equipped with one laser operating at 670 nm wavelength (designated FR for Fixed Red since it only probes the companion cell). The designs of the cell array and of SODI have already been described in a number of previous publications [14]. The companion cell can be measured simultaneously with and independent from the ternary samples, but it was decided to do it in parallel with the cell #5 since they had a similar duration of 48 h. SODI is not permanently installed but rather assembled on demand inside the Microgravity Science Glovebox. After arrival of the cell array on the ISS, the SODI instrument was assembled and the control was handled by EUSOC.

2.2. Run description

The experimental procedure is the same for primary and companion cells. The timeline of a typical run consists of six steps of different duration in accordance with the Experimental Scientific Requirement (ESR) [15]:

- Unmonitored thermal homogenenisation
- Monitored thermal homogenenisation
- Temperature gradient build-up
- Soret 1
- Soret 2
- Soret 3

At the first step a uniform temperature T_0 is applied to a specific cell, in order to homogenize the sample under investigation by both temperature and concentration. Then the image acquisition system is switched on and the isothermal condition is checked by MZI. Then, a temperature difference ΔT is applied to the sample. As soon as the temperature difference is established, the three Soret separation steps begin. The MZI image acquisition rate changes from higher to lower according to the change from Soret 1 step to Soret 3. At the end of the Soret separation phase, the thermal gradient is removed and the temperature of the cell is brought back to the ambient temperature. The duration of the total Soret step (Soret 1 + Soret 2 + Soret 3) has been estimated on the basis of available literature data, by calculating the characteristic diffusion time from the smaller eigenvalue of the diffusion matrix. In some cases, when no reference data was available, the timing was defined with some safety margins. At the end, the runs with different cells had very different duration, from several hours to a few days. The experimental run terminates at the end of the Soret 3 step.

2.3. Image logistic

The 5-steps phase-shifting interferometry technique implemented with SODI, needs in acquiring a set of 5 images phase-shifted by $\pi/2$ between them stored in the so-called "stack" format (.stk). Each stack filename contains the current cell, laser and timestamp. A selected set of files in each run was downloaded by telemetry, at the end of the run, and then delivered to the scientific team by ftp server connexion. Per run, two housekeeping files (.csv) contain driving current, temperature of three laser diodes and temperature of the top and bottom blocks of all six experimental cells. The experiments were monitored by the science team based on the assessment of the quality of these downloaded images. In Fig. 2 one can find an example of raw images contained in a stack. After mission completion all the image data were delivered via ftp, but in fits format (Flexible Image Transport System) which groups ten images for cells 1 to 4 (five consecutives images for MN laser + five consecutives images for MR laser) and fifteen images for cells 5 and 6 (five consecutive images for MN laser + five consecutive images for MR laser for cell 5 and five consecutive images for FR laser for cell 0). The total number of fits files received per run and per cell can be found in Tables 2–6.

3. Evaluation of optical data

Before extraction of required phase information from interference images, their quality has to be individually and independently estimated.

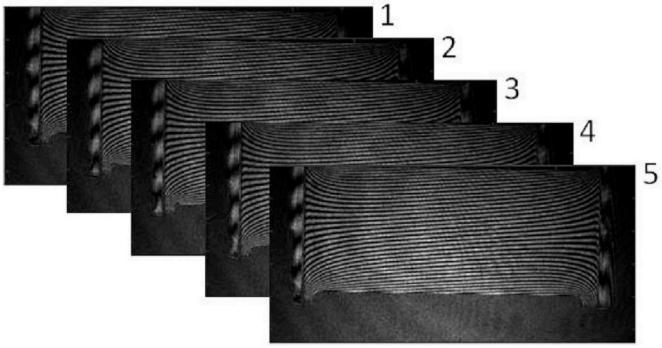

Fig. 2. The set of 5 fringes images for the 1_5_F691@0016_MN_DSC_190101_074147_5.stk file (run 5r01, cell #5, laser MN, Temperature gradient build-up step).

3.1. Image contrast

The contrast of the individual fringe images is an important characteristic of the data quality. But a problem with the contrast is that it can be determined in many different ways. First, it has to be evaluated over the part of the image where fringes are well developed. The ESR recommends for the contrast calculation to crop a central part of the fringe image with 20% of the width and 60% of the height of the original image [15,16]. We have found though, that to fall into the transparent Region Of Interest (ROI) of the liquid bulk, this central part has to be shifted by 100 pixels to the top of the image, as shown in Fig. 3. For the contrast estimations we have used this position of the central part, which always falls into cells ROI, for all lasers, cells and runs.

After selecting the proper ROI, we have tested different options for the contrast estimation. We started with a basic definition:

$$C = \frac{I_{max} - I_{min}}{I_{max} + I_{min}} \tag{1}$$

where I_{max} and I_{min} are maximal and minimal grey levels in the central part of the image, respectively. We have found, however, that such definition of the contrast provides strongly overestimated values in many cases. An example demonstrating the problem is shown in Fig. 4.

It clearly follows from the left pane of Fig. 4, that I_{max} and I_{min} levels automatically detected from the central part of the fringe image (shown by black dashed lines in the plot) are badly correlated with the vertical intensity profile taken across the central part. It happens because of saturated pixels may always be present in the image; and even the presence of very few of them can shift the top limit higher and the bottom limit lower, respectively. Another problem in the contrast calculation according to Eq. (1) is that if, by some reason, the minimum found grey level is $I_{min} = 0$ (even for a single pixel), the contrast equals to unity, independently of I_{max} value. To avoid these serious drawbacks of the basic definition, we suggest an improved definition, according to which the limiting grey levels are calculated as follows: I_{min} is an average over 20% of the total pixels counts featuring lowest graylevels. I_{max} is an average over 20% of the total pixels counts featuring highest graylevels, respectively. As it is seen in the left pane of Fig. 4, the improved definition (shown by blue dashed lines) does better match to the intensity profile of the fringe image. Correlation of the limiting graylevels detected according to both definitions with the image histogram is shown on right pane of Fig. 4.

There exist another way to calculate the contrast, which utilises the fact that at each pixel of the image the intensity has to pass from minimum to maximum during the cycle of the laser current steps. In this method the I_{min} and I_{max} values are calculated pixel-wise from all 5 fringe images of the stack shown in Fig. 5, and then averaged over the selected region:

$$C_M^i = \frac{1}{N_y' N_z'} \cdot \sum_{y=1}^{N_y'} \sum_{z=1}^{N_z'} \frac{I_{max}(y,z) - I_{min}(y,z)}{I_{max}(y,z) + I_{min}(y,z)} \tag{2}$$

Here N_y' is the number of pixels along the horizontal direction in the central area, and N_z' the number along the vertical direction. Result of the maximum and minimum graylevel detection by this method is shown in Fig. 5.

It seems that this method provides a good estimate for the average contrast over the stack. After determination of the contrast for each stack, it can be averaged over a run:

$$C_M = \frac{1}{N_S} \cdot \sum_{i=1}^{N_S} C_M^i \tag{3}$$

where N_S is the number of stacks in a run. For quantitative comparison of all the listed contrast calculation methods we have compiled the results of their application in Table 7, taking as a reference the same stack discussed in Figs. 4 and 5.

A brief overview of Table 7 suggests that the basic definition provides too optimistic estimates of the contrast, which often reach the unity value and only weakly reflect the real contrast drops (as seen in Fig. 5). This optimistic estimate does also lead to the wrong conclusion about absence of the mode hopping in the stack (since maximum deviation from the average contrast does not exceed 20%, according to this method). On the contrary, the improved definition (similar, but with the different way of detecting maximum and minimum levels) in some cases gives the contrast value twice lower; but it seemingly better reflects the contrast drops in some fringe images, and clearly indicates the presence of mode hopping during the stack acquisition. This way may be considered as a conservative estimate of the contrast. Third method provides an intermediate estimate for the average contrast in stack, which can be done faster, but it is not able to automatically detect the mode hopping on the basis of the contrast jumps within one stack.

We have systematically applied first two definitions to screen all the downloaded “fits” files for all the lasers with respect to the percentage of stacks affected by the mode hopping. We suggest considering the run/laser as seriously affected by mode hopping if the total number of

Table 2
Relevant parameters of the runs on cell 1, ternary mixture of toluene-methanol-cyclohexane in % mass fractions of 20-25-55.

run_#	run_{ID}	number of “fit” files	Soret step duration, h	$\langle T_0 \rangle$, K	σ_{T_0}, K	t_{grad}, s	$\langle \Delta T \rangle$, K	$\sigma_{\Delta T}$, K	t_{spikes}, s	RMS spikes	low frequency alert*
3	1r01	468	24	20.00	0.002	110	2.000	0.004	0.5	n/a	n/a
6	1r02	468	24	25.00	0.007	113	2.000	0.012	39.0	n/a	n/a
8	1r03	468	24	30.00	0.003	112	2.000	0.007	0	n/a	n/a
21	1r04	684	48	20.00	0.002	123	2.000	0.003	0	Y	Y
23	1r05	576	36	25.00	0.007	103	2.000	0.013	83.0	Y	Y
26	1r06	468	24	30.00	0.003	115	2.000	0.009	4.5	Y	Y
43	1r08	270	24	30.00	0.004	110	2.000	0.011	1.5	Y	Y
47	1r07	352	48	17.50	0.002	117	2.000	0.003	0	N	N
57	1r08d	270	20	17.50	0.002	n/a	0.000	n/a	n/a	Y	N

* band (0.17–0.35) Hz.

Table 3
Relevant parameters of the runs on cell 2, ternary mixture of toluene-methanol-cyclohexane in % mass fractions of 35-25-40.

run_#	run_{ID}	number of "fit" files	Soret step duration, h	$\langle T_0 \rangle$, K	σ_{T_0}, K	t_{grad}, s	$\langle \Delta T \rangle$, K	$\sigma_{\Delta T}$, K	t_{spikes}, s	RMS spikes	low frequency alert*
9	2r01	351	16	20.00	0.002	132	2.000	0.003	0	n/a	n/a
11	2r02	350	16	22.50	0.005	90	2.000	0.014	80.0	n/a	n/a
14	2r03	351	16	25.00	0.008	110	2.000	0.014	22.0	n/a	n/a
17	2r04	302	16	27.50	0.005	104	2.000	0.010	0	n/a	n/a
18	2r05	351	16	30.00	0.003	108	2.000	0.007	0	n/a	n/a
28	2r06	352	16	20.00	0.002	129	2.000	0.003	0	N	Y
34	2r07	352	16	22.50	0.004	107	2.000	0.011	17.5	Y	Y
36	2r08	352	16	25.00	0.007	98	2.000	0.015	102.0	Y	Y
38	2r09	352	16	27.50	0.006	112	2.000	0.007	1.0	n/a	n/a
40	2r10	352	16	30.00	0.004	122	2.000	0.010	3.5	n/a	n/a
45	2r11	468	16	20.00	0.002	124	2.000	0.003	0	N	Y
48	2r12	270	16	17.50	0.002	135	2.000	0.002	0	Y	N
50	2r13	352	24	15.00	0.001	133	2.000	0.002	0	Y	N
52	2r14	424	16	32.50	0.002	144	3.000	0.005	0	Y	N
54	2r15	352	16	35.00	0.002	145	3.000	0.004	0	Y	Y
56	2r16	352	24	13.00	0.001	145	2.000	0.001	0	Y	N

* band (0.17–0.35) Hz.

affected stacks exceeds 50%. Summary of the estimates is given in Table 8.

First, it is evident that the conservative estimate detects much more affected runs as compared with the optimistic one. While the optimistic estimate detects 6 run/laser combinations out of 121 in total, the conservative one finds 28. Second, only MR and FR lasers are found to be susceptible to the problem. Third conclusion is that the problem is seemingly not cell-dependent, but rather time-dependent, as there were some time intervals (between runs #16 … #28, and #28 … #40) where the problem was much less pronounced.

3.2. Phase stepping accuracy

Except the image contrast, which is more related to camera settings, there is another image characteristic, which is affected by the laser system. Due to the design of the interferometer, based on phase shift technique, and the specific way of its implementation, each laser has to often pass a set of steps with different driving currents. Five fringe images shown in Fig. 2 are then combined to one phase image. These dynamic operating conditions may lead to imperfect reproducibility of lasing regimes.

SODI utilises 5-steps algorithm with the step magnitude of $\omega_0 = \pi/2$. As a result, the periodic intensity profiles taken from individual fringe images of the same stack are evenly shifted with respect to each other such that 5th profile does coincide with 1st one. The usual approach for image analysis is to transform the 5 consecutive images for a laser at a given time stamp to one single phase image. This processing has successfully been implemented for DCMIX1 [2,17] and DCMIX2 [5]. There exists a broad literature on different algorithms for such image processing (usually defined as phase-shifting or phase-stepping interferometry), so one can choose the most suitable algorithm for the data at hand. One common algorithm for such a problem, also used for DCMIX1 and DCMIX2 data, is a variation of the "Hariharan's" algorithm [18]:

$$\Phi(y, z) = \arctan\left[\frac{7(I_4 - I_2)}{4I_1 - I_2 - 6I_3 - I_4 + 4I_5}\right] \quad (4)$$

Here Φ is the phase at the pixel of horizontal coordinate y and vertical coordinate z and $I_m = I(y, z)_m$ is the two-dimensional intensity information of the mth image in the group of 5. Due to the arctangent, these phase values Φ are wrapped to the interval $-\pi$ to $+\pi$. Therefore, a so-called phase unwrapping procedure has to be applied, which shifts the phase data to construct a continuous phase information. Due to the common nature of all experiments based on phase-shifting

Table 4
Relevant parameters of the runs on cell 3, ternary mixture of toluene-methanol-cyclohexane in % mass fractions of 55-25-20.

run_#	run_{ID}	number of "fit" files	Soret step duration, h	$\langle T_0 \rangle$, K	σ_{T_0}, K	t_{grad}, s	$\langle \Delta T \rangle$, K	$\sigma_{\Delta T}$, K	t_{spikes}, s	RMS spikes	low frequency alert*
1	3r03	269	12	25.00	0.005	140	5.000	0.004	0	n/a	n/a
4	3r01	270	12	20.00	0.005	126	5.000	0.014	0	n/a	n/a
10	3r02	269	12	22.50	0.003	137	5.000	0.007	0	n/a	n/a
12	3r04	270	12	27.50	0.006	141	5.000	0.004	0	n/a	n/a
15	3r05	270	12	30.00	0.004	135	5.000	0.010	0	n/a	n/a
19	3r07	270	12	35.00	0.002	155	5.000	0.003	0	n/a	n/a
20	3r06	190	12	32.50	0.003	130	5.000	0.011	0	n/a	n/a
24	3r06r	270	12	32.50	0.005	122	5.000	0.012	17.0	Y	Y
30	3r08	270	12	20.00	0.004	121	5.000	0.014	0	N	Y
31	3r09	270	12	22.50	0.004	134	5.000	0.007	0	Y	Y
32	3r10	270	12	25.00	0.006	136	5.000	0.004	0	N	N
35	3r11	270	12	27.50	0.006	143	5.000	0.003	0	N	N
37	3r12	270	12	30.00	0.003	143	5.000	0.007	0	N	Y
39	3r13	270	12	32.50	0.004	126	5.000	0.014	0	N	N
41	3r14	270	12	35.00	0.002	134	5.000	0.005	0	Y	Y
44	3r15	468	12	17.50	0.002	143	5.000	0.003	0	N	N
46	3r16	270	12	15.00	0.002	141	5.000	0.003	0	N	N
51	3r17	1650	16	13.00	0.002	142	5.000	0.002	0	Y	Y
53	3r18	306	16	14.00	0.002	141	5.000	0.002	5.5	Y	N
55	3r19	306	12	37.50	0.002	156	5.000	0.003	0	N	N

* band (0.17–0.35) Hz.

Table 5
Relevant parameters of the runs on cell 4, ternary mixture of fullerene-tetralin-toluene in % mass fractions of 0.07-60-39.93

run_#	run_{ID}	number of "fit" files	Soret step duration, h	$\langle T_0 \rangle$, K	σ_{T_0}, K	t_{grad}, s	$\langle \Delta T \rangle$, K	$\sigma_{\Delta T}$, K	t_{spikes}, s	RMS spikes	low frequency alert*
2	4r01	467	24	25.00	0.016	123	5.000	0.023	0.5	n/a	n/a
5	4r02	466	24	30.00	0.010	131	5.000	0.011	0	n/a	n/a
7	4r03	468	24	35.00	0.003	142	5.000	0.005	0	n/a	n/a
22	4r04	468	24	20.00	0.012	103	5.000	0.035	1.0	N	Y
25	4r05	468	24	25.00	0.012	118	5.000	0.025	1.0	Y	Y
27	4r06	468	24	30.00	0.010	121	5.000	0.009	0	Y	Y
29	4r07	468	24	35.00	0.003	141	5.000	0.005	0	Y	Y
42	4r08	352	24	20.00	0.013	102	5.000	0.035	4.0	Y	Y

* band (0.17–0.35) Hz.

interferometry, this problem is widely known in the literature and many different approaches for phase-unwrapping exist.

As a result, the optical phase obtained from the set of 5 periodic intensity distributions by one of well established algorithms has to take a smooth (and in case of DCMIX, locally linear) shape. Examples of unwrapped phase can be seen in Fig. 6 on the right panels. In the case of violation of the phase step stability, this even spatial shift of the fringes intensity is disturbed, and the reconstructed optical phase distribution does notably deviate from the local linearity. While it is in principle feasible to detect exact relative phase step for each fringe image, this information does not have an explicit correlation with the resulting optical phase quality. We decide therefore to define the error on the phase calculation as the standard deviation $\sigma_{\Delta\Phi}$ of the difference $\Delta\Phi = \Phi_{un} - \Phi_{interp}$ between unwrapped experimental phase and its linear interpolation. In scientific requirements the threshold criteria for the phase error estimate are formulated as relative. Thus, the standard deviation of the phase has to be related to a total phase difference, which was not explicitly defined. After some tests we have found however, that a quality criteria can be introduced, formulated as the percentage of the standard deviation to 3 phase steps ratio:

$$Q_{PS} = \frac{\sigma_{\Delta\Phi}}{6\pi} \cdot 100\% \tag{5}$$

To illustrate the credibility of the proposed estimate we have selected some samples from a run that is least affected by contrast jumps (to avoid an interference with the mode hopping). Selected images of this run, featuring different values of the phase stepping quality, are presented in Fig. 6. The intensity profiles, calculated phase distribution and the quality estimate are done for a short vertical segment with length covering 3 phase steps and located in the center of the central part of the image (the ROI used for all image quality estimations). The raw intensity profiles presented on left side of Fig. 6 are slightly filtered to facilitate the visual localization of the extrema.

Obviously, the quality parameter Q_{PS} with magnitude less than 1.2% does correspond to almost linear phase distribution, with RMS $\sigma_{\Delta\Phi}$ only twice larger than a typical phase noise in interferometric measurements. Another threshold of 4% corresponds to approaching a limit where even accurate phase unwrapping may become difficult or even impossible. Interestingly, the phase steps in the last case shown in Fig. 6 were so messy that even the sign of the phase variation has been changed.

The complete information for all runs ordered chronologically is given in Fig. 7. The runs which $Q_{PS} < 1.2\%$ can be characterized as having good quality images and runs for which $Q_{PS} < 4\%$ have satisfactory quality. By screening all runs/lasers combinations we have found that the stacks of MR laser have been affected by the phase shifting errors most seriously. For MN laser the number of stacks per run which surpass the minimum threshold of 4% has never exceeded 1%, while MR laser in a set of runs produced more that 25% of stacks violating the minimum threshold. These runs are 4r02, 2r04, 2r05, 3r07, 3r06, 2r12 and 2r16 are the ones closest to the horizontal dotted line in Fig. 7.

3.3. Optical saturation

Images recorded by SODI have a resolution of 1920 × 1080 pixels (Fig. 3) by laser and by camera, with 256 intensity graylevels per pixel. Too many saturated pixels in the white or the black can lead to a loss of information. According to ESR, this number must not exceed per image in the white and the in black a minimum of 5%, with an optimum of 1%.

For all the images we have verified that the optimum of 1% is reached on the white saturation. In the central part of the images, we verified that the mimimun of 5% was reached on the black saturation.

4. Temperature control

Stability of the thermal regulation is one of the important characteristics in a thermodiffusion experiment. We have carefully examined it over all the runs of DCMIX4 experiment. A typical temperature record of one run is shown in Fig. 8.

The record of an experiment combines readings from two sensors incorporated in the top and bottom plates of the cell, and in the

Table 6
Relevant parameters of the runs on cell 5, ternary mixture of polystyrene-toluene-cyclohexane in % mass fractions of 2-39-59 and in parentheses on the cell 6, binary mixture of polystyrene-toluene in % mass fractions of 2–98.

run_#	run_{ID}	number of "fit" files	Soret step duration, h	$\langle T_0 \rangle$, K	σ_{T_0}, K	t_{grad}, s	$\langle \Delta T \rangle$, K	$\sigma_{\Delta T}$, K	t_{spikes}, s	RMS spikes	low frequency alert*
13	5r01	1647	48	20.00 (20.00)	0.006 (0.004)	117 (117)	5.000 (5.000)	0.018 (0.014)	21.5 (0)	n/a	n/a
16	5r02	1482	48	25.00 (25.00)	0.007 (0.007)	138 (138)	5.000 (5.000)	0.004 (0.004)	11.5 (0.5)	n/a	n/a
33	5r03	1650	48	30.00 (30.00)	0.003 (0.003)	141 (142)	5.000 (5.000)	0.007 (0.007)	0 (0)	Y	Y
49	5r04	1650	48	35.00 (35.00)	0.003 (0.004)	139 (134)	5.000 (5.000)	0.006 (0.007)	0 (0)	Y	Y
58	5r02r	1650	48	25.00 (25.00)	0.005 (0.006)	151 (149)	5.000 (5.000)	0.004 (0.004)	0 (0)	Y	Y

* band (0.17–0.35) Hz.

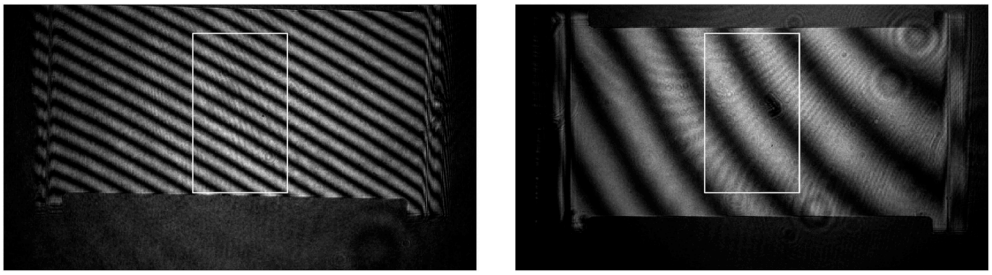

Fig. 3. Selection of the central part of the fringe image for MR (left) and FR (right) lasers. Stack #20 of the thermalization step of the run 5r01.

DCMIX4 experiment it consists of three temporal parts: (1) thermalization step (interval from 0 to 24 h in Fig. 8), (2) short gradient build-up step, and (3) Soret step (interval from 24 to 60 h in Fig. 8). We did not characterize the records of individual sensors; instead, we looked at the behaviour of the more important composite parameters, like the mean temperature, $T_0 = (T_{top} + T_{bot})/2$, and the temperature difference, $\Delta T = T_{top} - T_{bot}$. In Tables 2–6, we present values of the averaged mean temperature $\langle T_0 \rangle$, and its standard deviation σ_{T_0} calculated over complete run duration by cell. In the same manner we characterize the averaged temperature difference $\langle \Delta T \rangle$, and its standard deviation $\sigma_{\Delta T}$, but calculated over Soret step only. We also calculated an exact duration of the transition (gradient build-up) step. It is another important parameter, as this duration should be as short as possible to obtain cleaner results. The principle of determining the transition time t_{grad} is presented in Fig. 9. It is calculated as a time between the depart of the record from the RMS interval around the mean temperature and the time instant when it enters the RMS interval around $\langle \Delta T \rangle$. The corresponding points are marked by black crosses in Fig. 9.

It is seen in Table 2–6 that this transition time was relatively short in all runs, varying from 1.5 to 2.5 min. The most crucial problem is the stability of the temperature difference over the Soret step. In addition to the temperature jitter appearing due to the active thermal regulation and characterized by RMS of ΔT, there are also some disturbances, short in time, but with larger amplitude, so called spikes or surges. Such spikes may completely corrupt the data from images which are falling in the same time interval. For all the runs we have calculated total time duration covered by such spikes during the Soret steps. The way of calculating the time of a spike is illustrated in Fig. 10. We first define a safety margin for the temperature difference, $\delta(\Delta T)$, and calculate the cumulative time during which the record is running out of this margins.

As a primary measure of the margin we took ten times RMS of the temperature difference, $10\sigma_{\Delta T}$. But since the RMS was elevated in many runs (see Tables 2–6), we applied an additional limit, 2% of ΔT. Thus, the complete definition of the margin is $\delta(\Delta T) = min\{10\sigma_{\Delta T}, 0.02\Delta T\}$. It

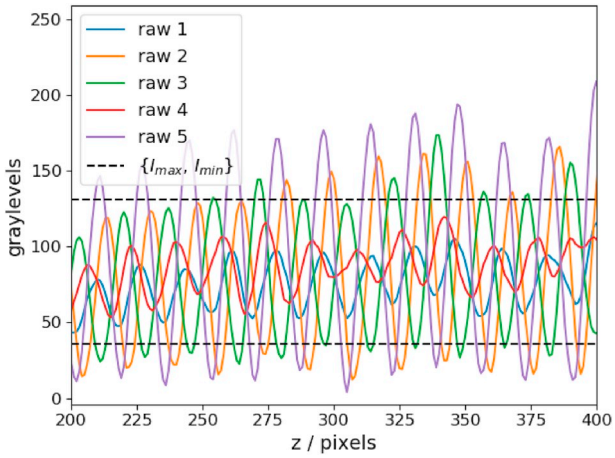

Fig. 5. Determining the contrast by all 5 fringe images of stack. I_{max} and I_{min} graylevels are obtained by averaging over the plotted vertical intensity profiles. The raw data are taken from the same stack as in Fig. 4. (For interpretation of the references to color in this figure legend, the reader is referred to the Web version of this article.)

is seen from Tables 2–6, that even in worst cases the time of Soret steps disturbed by the temperature surges does not exceed 100 s, which limits the probability for the images to be corrupted due to thermal disturbances. At the same time, many runs feature relatively high thermal jitter, $\sigma_{\Delta T} > 0.01K$. It is important to note that a comparative analyses of RMS ($\sigma_{\Delta T}$) in different cells did not provide any preference between the cells. However, we noticed that the increase in RMS depends on days and is most likely associated with activity on the ISS.

5. Vibrational characterization

Because of a limited amount of data available for post-flight analysis

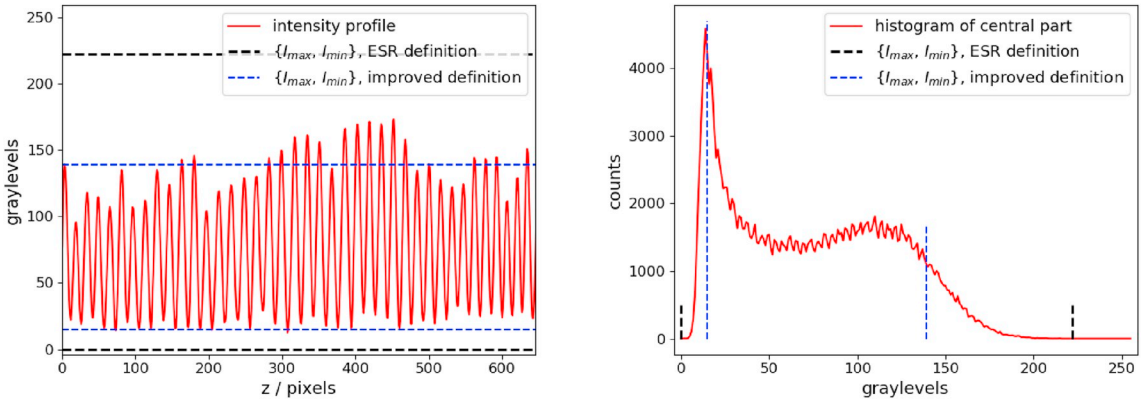

Fig. 4. Determining of I_{max} and I_{min} grey levels for the contrast estimation. Correlation of these levels with the vertical intensity profile along vertical center line of the central part of the fringe image (left) and with the histogram of the central part (right). Run 4r01, MR laser, stack #118 (Soret 1 step), raw #2. (For interpretation of the references to color in this figure legend, the reader is referred to the Web version of this article.)

Table 7
Results of the contrast calculation according to different methods. Run 4r01, MR laser, img#118 (soret1 step).

Calculation method	raw 1	raw 2	raw 3	raw 4	raw 5	average	max. dev, %	mode hopping
ESR	0.74	1.00	0.93	0.71	1.00	0.88	19	no
Improved	0.34	0.81	0.67	0.30	0.89	0.60	49	yes
Stack-averaged	n/a	n/a	n/a	n/a	n/a	0.82	n/a	n/a

Table 8
List of run/laser combinations which are seriously affected by mode hopping (more than 50% of stacks affected), according to different definitions of the contrast.

run_#	run_{ID}	$laser_{ID}$	ESR	Improved
1	3r03	MR		+
2	4r01	MR	+	+
5	4r02	MR	+	+
6	1r02	MR		+
8	1r03	MR		+
9	2r01	MR		+
10	3r02	MR		+
11	2r02	MR		+
12	3r04	MR		+
13	5r01	MR		+
13	5r01	FR		+
14	2r03	MR	+	+
15	3r05	MR		+
16	5r02	MR		+
16	5r02	FR		+
28	2r06	MR		+
40	2r10	MR		+
43	1r08	MR		+
44	3r15	MR	+	+
45	2r11	MR	+	+
47	1r07	MR		+
48	2r12	MR		+
49	5r04	FR		+
50	2r13	MR		+
55	3r19	MR	+	+
56	2r16	MR		+
57	1r08d	MR		+
58	5r02r	FR		+

and the absence of possibility to repeat the experiment, it is important to clarify all unknown sources of errors. Perturbations of some microgravity experiments is usually attributed to the effect of the residual accelerations environment. The recent study [19] showed the daily onboard environment of the ISS does not interfere with diffusion controlled experiments. However, the transient (pulse-like) acceleration of external forces (docking, orbit correction, etc.) may affect the diffusion-controlled processes depending on the duration of the pulse [20,21]. Regularly, accelerometric data are analyzed only for a few runs per experiment [22,23].

To carry out the vibrational analisys we used acceleration data coming from the nearest sensor to the experiment, the es09006. This sensor was located inside the Microgravity Science Glovebox (Destiny module). The raw acceleration signals, with a sampling rate of 142 Hz and a cut-off frequency of 6 Hz, were freely downloaded from PIMS NASA website (https://gipoc.grc.nasa.gov/wp/pims/home/). Additional information about the various events occurred during different runs were provided us by the EUSOC, who made a preliminary evaluation of the signal completion. In Tables 2–6, one can find details related to the sensor operation. Note, the acceleration data of the first 20 runs were unavailable and the signals corresponding to the runs 2r09 and 2r10 were also incomplete. This high insufficiency rate is aggravated because all runs had a missing data interval when passing from one day to another. The signal recordings were systematically stopped during 10 min after midnight. The available accelerometric information of the whole DCMIX4 experiment is thus incomplete and contains only 59%. Note that the acceleration signals of the last ten runs, between 18th February and 4th March, were recorded with a sampling rate of 500 Hz and filtered at 200 Hz. A complementary low-pass filtering was then effected to homogenize all signals preserving frequency information below 6 Hz.

Digital signal processing techniques used to analyse all available data were systematically applied minute by minute covering both time and frequency domain. The first approach in time domain was the 1-min Root Mean Square (RMS) acceleration. This RMS highlights the oscillatory content of the acceleration signal, readily visualizing large sudden variations against the mean value or spikes. In previous works we have identified a warning spike when its RMS value exceeds 20% of the mean of all RMS values of the signal [24]. In these cases, the experimentalists should take them into account when interpreting doubtful experimental results, if any. Tables 2–6, indicate the runs in which spikes were detected. The Power Spectral Density (PSD) and warning maps based on the RMS values evaluated over one-third octave frequency bands [24,25] were used. As the signals were filtered to 6 Hz, this characterization focuses on the low frequency range which it is known to be the most harmful for the thermodiffussion experiments. RMS warning maps are two-dimensional tools that quickly visualize if the ISS vibratory limits were surpassed all along the experiment. Tables 2–6 show all problematic low frequency ranges for the analyzed runs.

6. Summary and conclusions

As part of the 4th campaign on the DCMIX project, thermodiffusion experiments on 3 compositions of the toluene-methanol-cyclohexane ternary mixture, on a mixture of fullerene-tetralin-toluene and on a mixture of polystyrene-toluene-cyclohexane have been performed in microgravity conditions on board the International Space Station. A binary mixture of polystyrene-toluene has been filled into the companion cell for the campaign. In order to obtain the temperature and the concentration fields in the cells, a two-wavelength Mach-Zehnder interferometer (MR and MN lasers) has been used for the ternary mixtures and a monochromatic Mach-Zehnder interferometer (FR laser) for the binary mixture. Precisely, the 5-steps phase-shifting interferometry technique which is implemented with SODI, with $\pi/2$ stepping has been utilized in SODI.

A total of 58 runs of various durations and at different mean temperatures have been conducted. The experiments in the companion cell were carried out in parallel with the polymeric ternary mixture since they had a similar duration of 48 h. Prior to any determination of diffusion and Soret coefficients, the quality of the recorded measurements must be evaluated. In order, we have analyzed the contrast of the interferograms, the regularity in the step shifting magnitude, the stability in the thermal regulation and the level of environmental disturbances on board the space station during the campaign.

Based on the Michelson contrast definition, we have tested different possibilities, distinct in a way of I_{min} and I_{max} determining. The

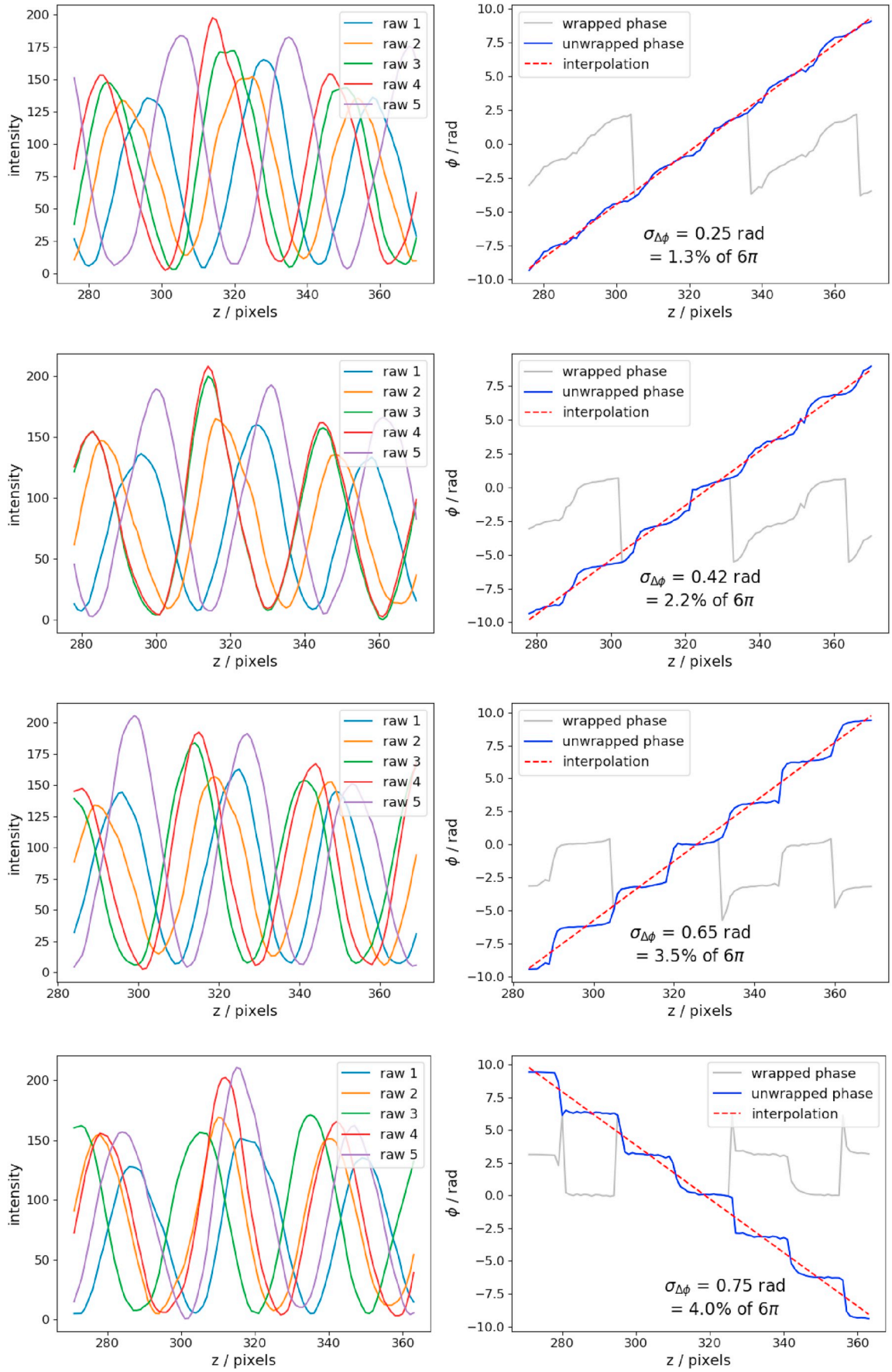

Fig. 6. Determining of the quality in the phase shift. Examples are taken from run 2r05, MR laser, Soret1 step, stacks #26, 30, 58 and 29 (from top to bottom). (For interpretation of the references to color in this figure legend, the reader is referred to the Web version of this article.)

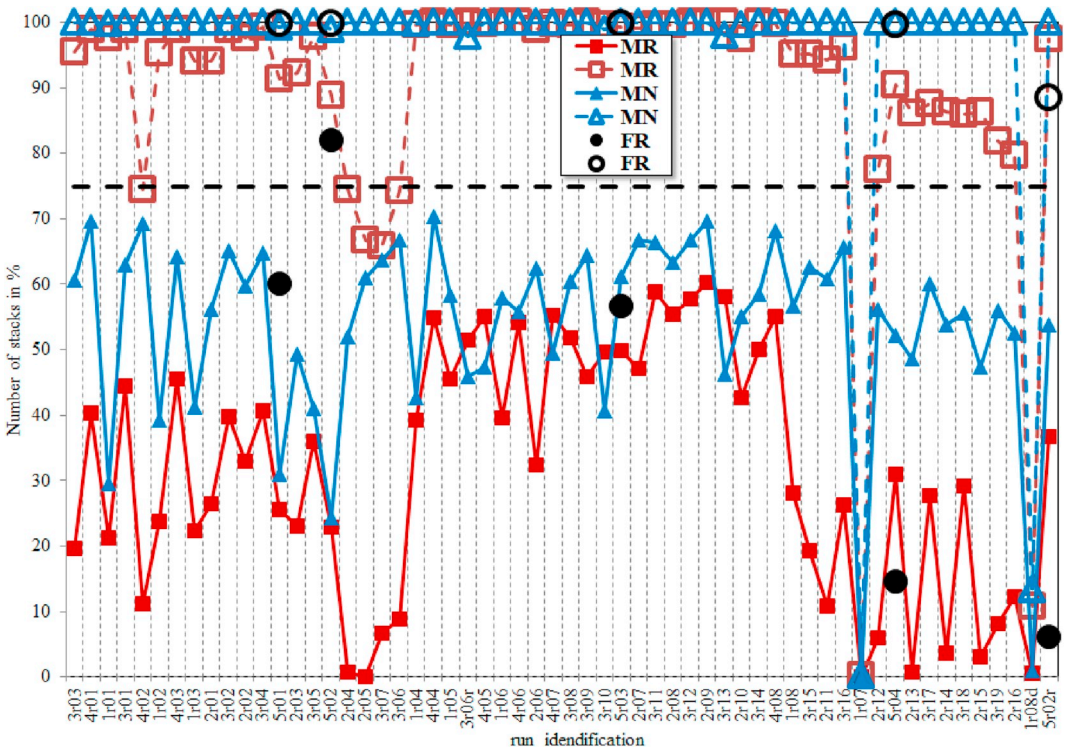

Fig. 7. Number of stacks in % over all the dowloaded "fit" files in the entire run for which $Q_{PS} < 1.2\%$ (filled red squares for MR laser, filled blue triangles for MN laser, filled black circles for FR laser) and $Q_{PS} < 4\%$ (empty red squares for MR laser, empty blue triangles for MN laser, empty black circles for FR laser). (For interpretation of the references to color in this figure legend, the reader is referred to the Web version of this article.)

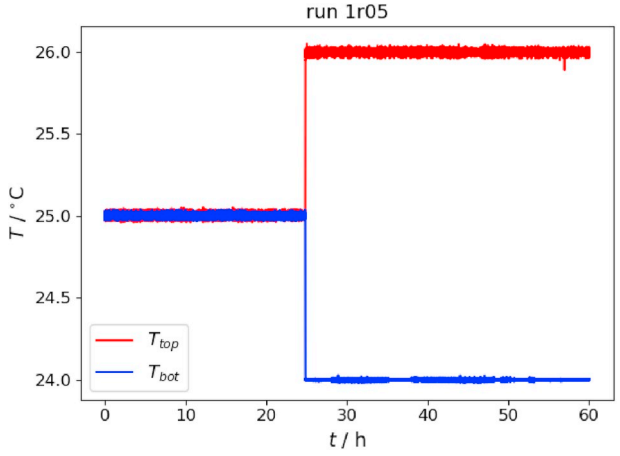

Fig. 8. Full temperature record of run 1r05. (For interpretation of the references to color in this figure legend, the reader is referred to the Web version of this article.)

approach, proposed here, allowed us to characterize the contrast, and its jumps within a stack of interferograms (lasers mode hopping) more accurately. We have found 28 run/laser combinations affected out of 121, and which are listed in Table 8. Another important observation is that only MR and FR lasers are prone to this problem. It was also noted that the problem, apparently, does not depend on the cell, but rather depends on the time, since some time intervals were determined.

To characterize the quality of the phase stepping, we make use of the fact of a local linearity (continuity and absence of extrema) of the optical phase observed in DCMIX experiments. The phase stepping problem is immediately recognized as a violation of the linearity. Then, an obvious estimate is a magnitude of deviation from an interpolation line. Based on this principle, we have suggested a phase-stepping quality parameter, quantitatively consistent with the experimental scientific requirements. The threshold, corresponding to 4% magnitude of the parameter, marks a limit when the optical phase reconstruction by the phase-stepping becomes impossible. After screening of all runs, we have identified seven runs where more than 25% of the stacks do violate this threshold. For these runs we recommend to use algorithms based on the analysis of a single image for the optical phase extraction. The FR laser shows a decrease in the stepping quality on its last run.

Stability of the thermal regulation is one of the important characteristics in a thermodiffusion experiment. Using the temperature records, we estimated the mean temperatures, the applied temperature differences and their standard deviations. There are conform to the expected values with a stability of the mK. The durations of the gradient build-up were relatively short in all runs, varying from 1.5 to 2.5 min. The temperature differences were stable to one hundredth of Kelvin, with small spikes that did not exceed 2 min and only for 3 runs. Sudden disturbances during the runs were detected and pointed out in Tables 2–6. All these effects are therefore perfectly negligible for DCMIX4 experiment.

Due to the inherent mode of operation of the ISS, vibrations at low frequencies are present in all experiments on board the space station. Exceeds within the ISS authorized limits were also identified in Tables 2–6.

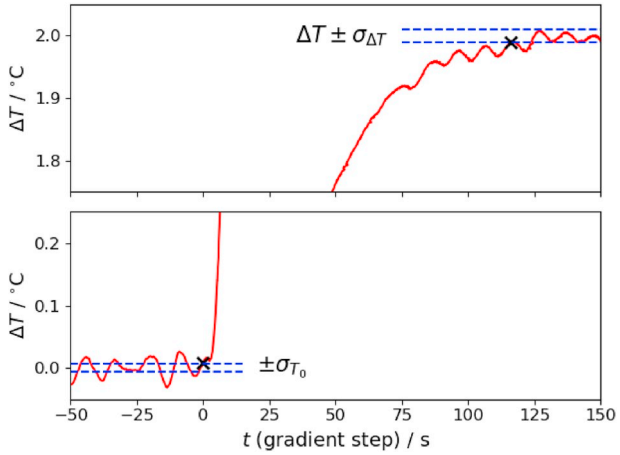

Fig. 9. Determining of the duration of the gradient build-up step (run 1r02).

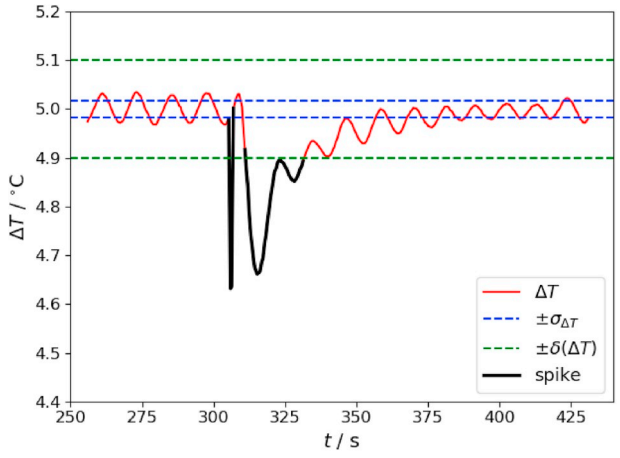

Fig. 10. Example of the thermal spike (from run 5r01). Time duration is calculated for the record when it is running out of the safety margins. The margins are plotted dashed green while the corrupted part of the record is painted black. (For interpretation of the references to color in this figure legend, the reader is referred to the Web version of this article.)

The raw DCMIX4 data will be available for public access as from June 2020 connecting to the address https://hreda.esac.esa.int/hreda/#/pages/home and following the instructions.

Declaration of competing interest

The authors declare that they have no known competing financial interests or personal relationships that could have appeared to influence the work reported in this paper.

Acknowledgements

This work has been developed in the framework of the cooperative project DCMIX (No. AO-2009-0858/1056) of the European Space Agency and the Russian Space Agency (Roscosmos)/TsNIIMash. AM, QG, YG, VS, SVV and VY acknowledge support from the PRODEX program of Belgian Federal Science Policy Office (BELSPO). The Mondragon group acknowledges the support of the ATNEMFLU program (ESP2017-83544-C3-1-P) of the MINECO project from Spain and MMMfavIN (KK-2020/00099) of the Basque Government. FC, LGF and HB acknowledge support from the French Center Nationale d'Etudes Spatiales (CNES). FC and HB also acknowledge that the project leading to this publication has received funding from the I-Site E2S Excellence Initiative of the Université de Pau et des Pays de l'Adour, a French "Investissements d'Avenir" program managed by ANR (ANR-16- IDEX-0002). The Bayreuth group acknowledges support from the Deutsches Zentrum für Luft- und Raumfahrt (DLR grant 50WM1544). Research at Complutense University is further supported by the Research grant ESP2017-83544-C3-2-P of the Spanish Agencia Estatal de Investigación. The URV group acknowledges the support of the Research grant ESP2017-83544-C3-1-P (MCIU/FEDER).

References

[1] M.M. Bou-Ali, A. Ahadi, D. Alonso de Mezquia, Q. Galand, M. Gebhardt, O. Khlybov, W. Köhler, M. Larranaga, J.C. Legros, T. Lyubimova, A. Mialdun, I. Ryzhkov, M.Z. Saghir, V. Shevtsova, S. Van Vaerenbergh, Benchmark DCMIX1: Soret, thermodiffusion and molecular diffusion coefficients of the ternary mixture THN-IBB-nC12, Eur. Phys. J. E 38 (2015) 30.

[2] Q. Galand, S. Van Vaerenbergh, W. Köhler, O. Khlybov, T. Lyubimova, A. Mialdun, I. Ryzhkov, V. Shevtsova, T. Triller, Results of the DCMIX1 experiment on measurement of Soret coefficients in ternary mixtures of hydrocarbons under microgravity conditions on the ISS, J. Chem. Phys. 151 (2019) 134502.

[3] V. Shevtsova, C. Santos, V. Sechenyh, J.-C. Legros, A. Mialdun, Diffusion and Soret in ternary mixtures. Preparation of the DCMIX2 experiment on the ISS, Microgravity Sci. Technol. 25 (2014) 275–283.

[4] A. Mialdun, V. Shevtsova, Temperature dependence of Soret and diffusion coefficients for toluene-cyclohexane mixture measured in convection-free environment, J. Chem. Phys. 143 (2015) 224902.

[5] A. Mialdun, I. Ryzhkov, O. Khlybov, T. Lyubimova, V. Shevtsova, Measurement of Soret coefficients in a ternary mixture of toluene-methanol- cyclohexane in convection-free environment, J. Chem. Phys. 148 (2018) 044506.

[6] T. Triller, D. Sommermann, M. Schraml, F. Sommer, E. Lapeira, M.M. Bou-Ali, W. Köhler, The Soret effect in ternary mixtures of water + ethanol + triethylene glycol of equal mass fractions: ground and microgravity experiments, Eur. Phys. J. E 42 (2019) 27.

[7] D. Sommermann, T. Triller, M. Schraml, F. Sommer, E. Lapeira, M. Bou-Ali, W. Köhler, A robust data evaluation method for the DCMIX microgravity experiments, Microgravity Sci. Technol. 30 (2018) 295.

[8] A. Errarte, M.M. Bou-Ali, M. Aginagalde, C. Santamaria, Thermodiffusion coefficients of nanofluid binary mixtures, Microgravity Sci. Technol. 31 (2019) 877–882.

[9] R. Bakry, R.M. Vallant, M. Najam-ul-Haq, M. Rainer, Z. Szabo, C.W. Huck, G.K. Bonn, Preparation of fullerenes and fullerene-based materials, Int. J. Nanomed. 2 (4) (2007) 639–649.

[10] H. Bataller, T. Triller, B. Pur, W. Köhler, J.M. Ortiz de Zárate, F. Croccolo, Dynamic analysis of the light scattered by the non-equilibrium fluctuations of a ternary mixture of polystyrene-toluene-n-hexane, Eur. Phys. J. E 40 (2017) 35.

[11] F. Croccolo, L. García-Fernández, H. Bataller, A. Vailati, J.M. Ortiz de Zárate, Propagating modes in a binary liquid mixture under thermal stress, Physical Review E 99 (2019) 12602.

[12] L. García-Fernández, H. Bataller, J.M. Ortiz de Zárate, F. Croccolo, Coupled non-equilibrium fluctuations in a polymeric ternary, Eur. Phys. J. E 42 (2019) 124.

[13] A. Mialdun, H. Bataller, M.M. Bou-Ali, M. Braibanti, F. Croccolo, A. Errarte, J.M. Ezquerro, Yu. Gaponenko, L. García-Fernández, J.J. Fernández, J. Rodríguez, V. Shevtsova, Preliminary analysis of diffusion coefficient measurements in ternary mixtures 4 (DCMIX4) experiment onboard the International Space Station, Eur. Phys. J. E 42 (2019) 87.

[14] A. Mialdun, C. Minetti, Y. Gaponenko, V. Shevtsova, F. Dubois, Analysis of the thermal performance of SODI instrument for DCMIX configuration, Microgravity Sci. Technol. 25 (2013) 83–94.

[15] M. Braibanti, DCMIX4 Experiment Scientific Requirements, European Space Agency, 2018.

[16] T. Triller, H. Bataller, M.M. Bou-Ali, M. Braibanti, F. Croccolo, J.M. Ezquerro, Q. Galand, J. Gavaldà, E. Lapeira, A. Laverón-Simavilla, T. Lyubimova, A. Mialdun, J.M. Ortiz de Zárate, J. Rodríguez, X. Ruiz, I.I. Ryzhkov, V. Shevtsova, S. Van Vaerenbergh, W. Köhler, Thermodiffusion in ternary mixtures of water/ethanol/triethylene glycol: first report on the DCMIX3- experiments performed on the International Space Station, Microgravity Sci. Technol. 42 (2018) 27.

[17] A. Mialdun, J.-C. Legros, V. Yasnou, V. Sechenyh, V. Shevtsova, Contribution to the benchmark for ternary mixtures: measurement of the Soret, diffusion and thermodiffusion coefficients in the ternary mixture THN/IBB/nC12 with 0.8/0.1/0.1 mass fractions in ground and orbital laboratories, Eur. Phys. J. E 38 (2015) 27.

[18] B. Hariharan, F. Oreb, T. Eiju, Digital phase-shifting interferometry: a simple error-compensating phase calculation algorithm, Appl. Optic. 26 (1987) 2504.

[19] V. Shevtsova, Y.-A. Gaponenko, V. Sechenyh, D.-E. Melnikov, T. Lyubimova, A. Mialdun, Dynamics of a binary mixture subjected to a temperature gradient and

oscillatory forcing, J. Fluid Mech. 767 (2015) 290–322.
[20] R. Jurado, Jna. Gavaldà, M.J. Simon, J. Pallares, A. Laverón-Simavilla, X. Ruiz, V. Shevtsova, Some considerations on the vibrational environment of the DSC-DCMIX1 experiment onboard ISS, Acta Astronaut. 129 (2016) 345–356.
[21] R. Jurado, J. Pallares, Jna. Gavaldà, X. Ruiz, Effect of reboosting manoeuvres on the determination of the Soret coefficients of DCMIX ternary systems, Int. J. Therm. Sci. 142 (2019) 205–219.
[22] N. Saez, X. Ruiz, Jna. Gavaldà, J. Pallares, V. Shevtsova, Comparative ISS accelerometric analyses, Acta Astronaut. 94 (2014) 681–689.
[23] N. Saez, Jna. Gavalda, X. Ruiz, V. Shevtsova, Detecting accelerometric nonlinearities in the international space station, Acta Astronaut. 103 (2014) 16–25.
[24] J. Ollé, D. Dubert, Jna. Gavaldà, A. Laverón-Simavilla, X. Ruiz, V. Shevtsova, Onsite vibrational characterization of DCMIX2/3 experiments, Acta Astronaut. 140 (2017) 409–419.
[25] D. Dubert, J. Ollé, R. Jurado, Jna. Gavaldà, A. Laverón-Simavilla, X. Ruiz, V. Shevtsova, Characterization of the accelerometric environment of DCMIX2/3 experiments, Microgravity Sci. Technol. 30 (2018) 683–697.